

CLEO RESULTS ON TRANSITIONS IN HEAVY QUARKONIA ^a

T. SKWARNICKI

*Department of Physics, 201 Physics Building, Syracuse University
Syracuse, NY 13244, USA*



Recent CLEO results on electromagnetic and hadronic transitions in charmonium and bottomonium systems are reviewed.

1 Introduction

Heavy quarkonia states ($b\bar{b}$ and $c\bar{c}$) below the open flavor threshold live long enough that their excitation level can be changed by emission of a photon or soft gluons turning into light hadrons. The triplet- S states (n^3S_1) can be directly formed in e^+e^- annihilation at the electron-positron storage rings. Then the other excitations levels can be observed via one or more transitions (Fig. 1). The CLEO-III experiment ^{1,2} collected large $\Upsilon(1S, 2S, 3S)$ samples at the end of CESR operations at the $b\bar{b}$ threshold region (29, 9 and 6 million resonant decays respectively). These data samples are about a factor of 10 larger than previously available. Then the CESR beam energy was lowered to the $c\bar{c}$ threshold region. Three million $\psi(2S)$ resonant decays were recorded, split about equally between the CLEO-III and CLEO-c detectors (the latter has a small wire chamber replacing the CLEO-III silicon vertex detector). Even though this is not the world's largest sample, it is nevertheless unique, since CLEO is the first detector studying the charmonium system with excellent detection of both charged particles and photons. Excellent particle identification capabilities ² of the CLEO detector are also important for some results presented here.

2 Observation of $h_c(1^1P_1)$ State

Spin-spin forces in heavy quarkonia are predicted to be short-range. Thus, while significant hyperfine splitting is observed for charmonium S -states (e.g., 116 MeV for $n = 1$), the mass

^aPresented at 40th Rencontres De Moriond On QCD And High Energy Hadronic Interactions, 12-19 Mar 2005, La Thuile, Aosta Valley, Italy.

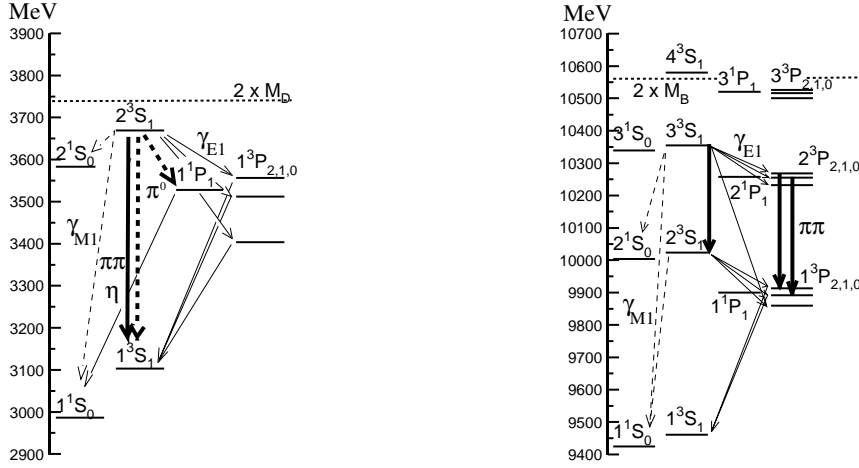


Figure 1: Various transitions in: (a) $c\bar{c}$ (left), and (b) $b\bar{b}$ (right) systems discussed in this article. The E1 (M1) photon transitions are indicated by the thin solid (dashed) lines. The $\pi\pi, \eta$ (π^0) transitions are indicated by the thick solid (dashed) lines.

splitting between the singlet state ($h_c(1^1P_1)$) and the center-of-gravity of the spin-triplet states ($\sum_J(2J+1)m(\chi_c(1^3P_J))/\sum_J(2J+1)$) is expected to be small. The $h_c(1^1P_1)$ was sighted previously twice in $\bar{p}p$ annihilation at two different masses³ with marginal statistical significance. Higher statistics searches disproved these observations. We present highly significant evidence for this state, settling the question about its mass.

We have observed the $h_c(1P)$ state in isospin violating π^0 transitions from the $\psi(2S)$ resonance, followed by a highly favored E1 photon transition, $h_c(1P) \rightarrow \gamma\eta_c(1S)$ (see Fig. 1a). Two essentially statistically independent approaches are used. In the inclusive approach, the $\eta_c(1S)$ is allowed to decay to anything. This approach results in a higher signal efficiency but also higher backgrounds. After imposing consistency of the reconstructed $\pi^0(\rightarrow \gamma\gamma)\gamma$ pair with the $\psi(2S)$ to $\eta_c(1S)$ transition, the π^0 -recoil mass is plotted (Fig. 2a). The photon four-vectors in the π^0 decay are constrained to the π^0 mass, substantially improving the recoil mass resolution. A peak of 150 ± 40 events, with a significance of 3.8 standard deviations, is observed.

In the second, exclusive, approach the $\eta_c(1S)$ is reconstructed in one of the following decay modes: $K_S^0 K^\pm \pi^\mp$, $K_L^0 K^\pm \pi^\mp$, $K^+ K^- \pi^+ \pi^-$, $\pi^+ \pi^- \pi^+ \pi^-$, $K^+ K^- \pi^0$, $K^+ K^- \eta(\rightarrow \gamma\gamma \text{ or } \rightarrow \pi^+ \pi^- \pi^0)$. Particle ID capabilities of the CLEO detector (RICH² and dE/dX) are critical in this analysis. The $\eta_c(1S)$ reconstruction was optimized on the hindered M1 photon transitions: $\psi(2S) \rightarrow \gamma\eta_c(1S)$ (see Fig. 1a). This approach results in excellent background suppression, but also in smaller signal efficiency. The π^0 -recoil mass for the exclusive analysis is plotted in Fig. 2b. A peak of 17.5 ± 4.5 events is observed at the mass consistent with the inclusive analysis. The probability of the background fluctuating up to produce this peak is equivalent to a signal significance of 6.1 standard deviations.

The average of the inclusive and exclusive mass measurements, $3524.4 \pm 0.6 \pm 0.4$ MeV, is $1.0 \pm 0.6 \pm 0.4$ MeV below the center-of-gravity of the $\chi_{cJ}(1P)$ states, confirming the conventional picture of spin-spin interactions. The measured product branching ratio, $\mathcal{B}(\psi(2S) \rightarrow \pi^0 h_c(1P)) \times \mathcal{B}(h_c(1P) \rightarrow \gamma\eta_c(1S)) = (4.0 \pm 0.8 \pm 0.7) \times 10^{-4}$, is in the midrange of the theoretical predictions⁴, which vary by 2 orders of magnitude due to difficulties in predicting the π^0 transition width.

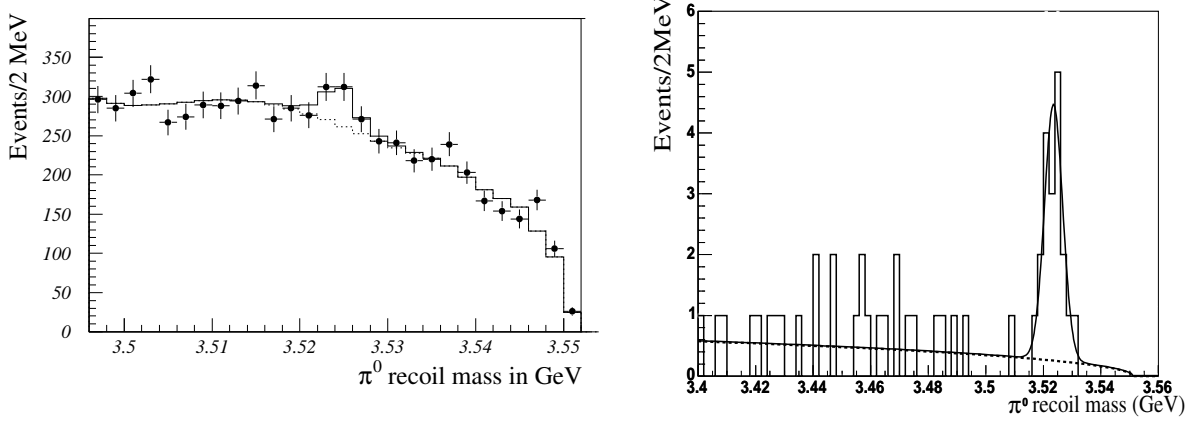


Figure 2: Recoil mass against the reconstructed π^0 in: (a) inclusive (left), and (b) exclusive (right) search for the h_c state. The fits are superimposed on the data.

3 Survey of $\psi(2S)$ to $J/\psi(1S)$ Transitions

We have performed a survey of $\psi(2S)$ to $J/\psi(1S)$ transitions, tagging J/ψ by its annihilation to electron or muon pairs (l^+l^-). The $\mathcal{B}(\psi(2S) \rightarrow XJ/\psi(1S))$ is measured from the J/ψ peak observed in the inclusive di-lepton mass distribution. Transition branching ratios for individual channels are measured by full reconstruction of the following exclusive event samples: $\pi^+\pi^-l^+l^-$, $\pi^0\pi^0l^+l^-$, $\eta(\rightarrow \gamma\gamma \text{ or } \rightarrow \pi^+\pi^-\pi^0)l^+l^-$, $\pi^0(\rightarrow \gamma\gamma)l^+l^-$, $\gamma\chi_{cJ} \rightarrow \gamma\gamma l^+l^-$ (see Fig. 1a). The backgrounds are small and dominated by feed-across between the transition modes. They are subtracted using Monte Carlo simulations. The large statistics, the small backgrounds and the large, well-understood detector acceptance result in the precision measurements. The results are compared to previous measurements in Table 1. A more detailed description of this analysis can be found elsewhere⁵. These are the most precise measurements to date. The difference between the inclusive and the sum over exclusive branching ratios is $(0.6 \pm 0.4)\%$, leaving little room for other, yet undetected modes. Unlike previous measurements, the $\pi^0\pi^0$ rate is half of the $\pi^+\pi^-$ rate, as expected from the isospin symmetry. The branching ratios for two-photon cascades via the $\chi_{c0,1}$ states are significantly higher than previously measured, which leads to significantly larger rates for $\chi_{c0,1} \rightarrow \gamma J/\psi$.

Channel	\mathcal{B} (%)			$\mathcal{B}/\mathcal{B}_{\pi^+\pi^-J/\psi}$ (%)	
	CLEO	PDG 2004	E835	CLEO	BES
$\pi^+\pi^-J/\psi$	$33.54 \pm 0.14 \pm 1.10$	31.7 ± 1.1	$29.2 \pm 0.5 \pm 1.8$		
$\pi^0\pi^0J/\psi$	$16.52 \pm 0.14 \pm 0.58$	18.8 ± 1.2	$16.7 \pm 0.5 \pm 1.4$	$49.24 \pm 0.47 \pm 0.86$	$57.0 \pm 0.9 \pm 0.3$
$\eta J/\psi$	$3.25 \pm 0.06 \pm 0.11$	3.16 ± 0.22	$2.8 \pm 0.2 \pm 0.2$	$9.68 \pm 0.19 \pm 0.13$	$9.8 \pm 0.5 \pm 1.0$
$\pi^0 J/\psi$	$0.13 \pm 0.01 \pm 0.01$	0.10 ± 0.02		$0.39 \pm 0.04 \pm 0.01$	
$\gamma\chi_{c0} \rightarrow \gamma\gamma J/\psi$	$0.18 \pm 0.01 \pm 0.02$	0.10 ± 0.01		$0.55 \pm 0.04 \pm 0.06$	
$\mathcal{B}(\chi_{c0} \rightarrow \gamma J/\psi)$	2.0 ± 0.3	1.2 ± 0.1			
$\gamma\chi_{c1} \rightarrow \gamma\gamma J/\psi$	$3.44 \pm 0.06 \pm 0.13$	2.67 ± 0.15		$10.24 \pm 0.17 \pm 0.23$	$12.6 \pm 0.3 \pm 3.8$
$\mathcal{B}(\chi_{c1} \rightarrow \gamma J/\psi)$	37.9 ± 2.2	31.6 ± 3.3			
$\gamma\chi_{c2} \rightarrow \gamma\gamma J/\psi$	$1.85 \pm 0.04 \pm 0.07$	1.30 ± 0.08		$5.52 \pm 0.13 \pm 0.13$	$6.0 \pm 0.1 \pm 2.8$
$\mathcal{B}(\chi_{c2} \rightarrow \gamma J/\psi)$	19.9 ± 1.3	20.2 ± 1.7			
XJ/ψ	$59.50 \pm 0.15 \pm 1.90$	57.6 ± 2.0		$1.77 \pm 0.01 \pm 0.02$	$1.87 \pm 0.03 \pm 0.06$

Table 1: The CLEO results⁵ for $\psi(2S)$ to $J/\psi(1S)$ transitions compared to the PDG fit values⁶ and two recently published measurements by BES⁷ and E835⁸.

Region	N_{bgd}	N_{obs}
di-pion sample		
other-backgrounds	37.6 ± 5.8	36
$\Upsilon(2S)_{\text{bgd}}$	7.6 ± 1.9	10
signal	1.2 ± 0.2	7
single-pion sample		
other-backgrounds	11.3 ± 2.6	13
$\Upsilon(2S)_{\text{bgd}}$	19.4 ± 4.9	26
signal	3.3 ± 0.7	17

Table 2.: The results for $\chi_b(2P) \rightarrow \pi^+\pi^-\chi_b(1P)$. Number of the observed (N_{obs}) and estimated background events (N_{bgd}) are given in the other-backgrounds, $\Upsilon(2S)_{\text{bgd}}$ and signal regions (see the text).

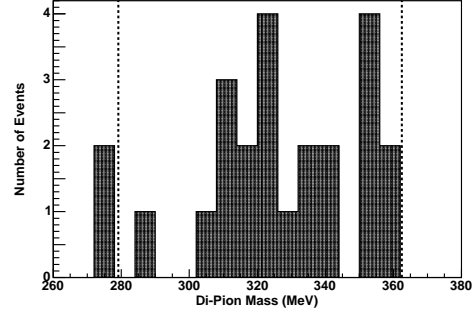


Figure 3: Distribution of $M(\pi^+\pi^-)$ for selected $\chi_b(2P) \rightarrow \pi^+\pi^-\chi_b(1P)$ events (di-pion and single-pion samples together). The dashed lines show the kinematic limits. The estimated background level is 4.5 ± 0.7 events (19%).

4 First Evidence for $\chi_b(2P) \rightarrow \pi^+\pi^-\chi_b(1P)$ Transitions

The $\pi^+\pi^-$ transitions have been previously observed in the $b\bar{b}$ system between the n^3S_1 states ($n = 1, 2, 3$). Such transitions are also expected among the n^3P_J states. We are presenting the first evidence for these transitions. The $\chi_b(2^3P_{J_2})$ states are produced by the E1 photon transitions from the $\Upsilon(3S)$ resonance (see Fig. 1b). The $\chi_b(1^3P_{J_1})$ states are recognized by E1 photon transition to the $\Upsilon(1S)$, followed by annihilation to l^+l^- . We look for the $\pi^+\pi^-$ transitions for $J_2 = J_1 = 1$ or 2, which are expected to have the largest rate. The dominant backgrounds come from the other transitions in the $b\bar{b}$ system, $\Upsilon(3S) \rightarrow \pi^+\pi^-\Upsilon(2S)$, $\Upsilon(2S) \rightarrow \gamma\chi_{bJ}(1P)$, $\chi_{bJ}(1P) \rightarrow \gamma\Upsilon(1S)$ (hereafter $\Upsilon(2S)_{\text{bgd}}$) in particular (see Fig. 1b). The fully reconstructed $\gamma\pi^+\pi^-\gamma l^+l^-$ events provide good background suppression but suffer from the small signal efficiency ($\epsilon \sim 4.5\%$), since the soft pions often curl-up and escape detection in the tracking system. Therefore, we have also selected events with only one detected pion ($\epsilon \sim 8.7\%$). For the di-pion events we define the signal, $\Upsilon(2S)_{\text{bgd}}$ and other-backgrounds regions by cuts on the energy of the lower-energy photon (identifying the $\chi_b(2P_{1,2})$ states) and the $\gamma_{\text{low}}\pi^+\pi^- - \gamma_{\text{low}}$ recoil mass-difference (identifying the $\chi_b(1P_{1,2})$ states). For the single-pion events the latter is replaced by a cut on the missing-mass of the event (reflecting the mass of the undetected pion). The observed event yields are compared to the estimated background rates in Table 2. After the background estimates are tuned to describe the observed background levels in the other-backgrounds sidebands, the observed event yields in the $\Upsilon(2S)_{\text{bgd}}$ regions are also well reproduced. In contrast, the signal region contains an excess of events, which corresponds to a statistical significance of 6 standard deviations. The $\pi^+\pi^-$ mass distribution in the signal region is plotted in Fig. 3. All results presented in this section are preliminary.

5 Photon transitions

We have analyzed inclusive photon spectra in the $\psi(2S)$, $\Upsilon(2S)$ and $\Upsilon(3S)$ data for monochromatic photons due to E1 and M1 photon transitions (see Fig. 1). The results have been published and can be found elsewhere⁹.

From the measurements of photon energies in the dominant E1 transitions, $n^3S_1 \rightarrow \gamma(n-1)^3P_{2,1,0}$, ratios of the fine splittings in the triplet- P states, $(M_2 - M_1)/(M_1 - M_0)$, are determined with a high precision: $0.490 \pm 0.002 \pm 0.003$ ($1P\ c\bar{c}$), $0.57 \pm 0.01 \pm 0.01$ ($1P\ b\bar{b}$) and $0.58 \pm 0.01 \pm 0.01$ ($2P\ b\bar{b}$). Somewhat surprisingly, the latter two are essentially equal.

In the non-relativistic limit, the E1 matrix elements for these transitions are J independent.

Thus, a ratio of the branching ratios ($\mathcal{B}(^3S_1 \rightarrow \gamma^3P_J)$) corrected for the phase-space factors ($((2J+1)E_\gamma^3)$) is expected to be 1 for any combination of J values. The results are summarized in Table 3. While the $(J=2)/(J=1)$ ratios in the $b\bar{b}$ system reproduce this expectation, the rates to the $J=0$ state are lower. Relativistic corrections were predicted to be, in fact, the largest for the transitions to 3P_0 state¹⁰. The ratios in the $c\bar{c}$ system are far from the non-relativistic prediction, apparently affected by the lighter quark mass and the $2^3S_1 - 1^3D_1$ mixing.

Final state	(J=2)/(J=1)	(J=0)/(J=1)	(J=0)/(J=2)
$\chi_b(2P)$	$1.00 \pm 0.01 \pm 0.05$	$0.76 \pm 0.02 \pm 0.07$	$0.76 \pm 0.02 \pm 0.09$
$\chi_b(1P)$	$1.01 \pm 0.02 \pm 0.08$	$0.82 \pm 0.02 \pm 0.06$	$0.81 \pm 0.02 \pm 0.11$
$\chi_c(1P)$	$1.50 \pm 0.02 \pm 0.05$	$0.86 \pm 0.01 \pm 0.06$	$0.59 \pm 0.01 \pm 0.05$

Table 3: Ratio of $\mathcal{B}(n^3S_1 \rightarrow \gamma(n-1)^3P_J)/(2J+1)E_\gamma^3$ as measured by CLEO for various J combinations in the charmonium and bottomonium systems.

The absolute values of the branching ratios are also significantly below the non-relativistic predictions for the $c\bar{c}$ system. Relativistic corrections are needed to explain the observed rates, as illustrated in Fig. 4a. In contrast, the relativistic correction in the $b\bar{b}$ system are not large and even non-relativistic calculations give a reasonable description of the data. This is true only for the dominant E1 transitions. The E1 matrix elements for the $^3S_1 \rightarrow \gamma 1^3P_J$ transitions are expected to be small, reflecting large cancellations in the integral of the dipole operator between the 3S_1 and 1^3P_J states. The relativistic corrections, and therefore the J dependence, are expected to be large. We have measured the $J=0$ rate for the first time. The theoretical predictions are scattered in a wide range and only a few models match our data well⁹.

While we have confirmed the hindered M1 transition $\psi(2S) \rightarrow \gamma\eta_c(1S)$, previously observed by Crystal Ball¹¹, their signal for the direct M1 transition $\psi(2S) \rightarrow \gamma\eta_c(2S)$ ¹² is not observed in our data. This is not surprising in view of the recent $\eta_c(2S)$ mass measurements¹³, which are inconsistent with the $\eta_c(2S)$ mass claimed by Crystal Ball. Searches for hindered M1 transitions in the $b\bar{b}$ system resulted in upper limits only, thus no singlet $b\bar{b}$ state has been observed to date. Only the most recent theoretical estimates of the expected M1 rates are consistent with all $c\bar{c}$ and $b\bar{b}$ data, and only marginally so with our limit on $\mathcal{B}(\Upsilon(3S) \rightarrow \gamma\eta_b(1S))$ (see Fig. 4b).

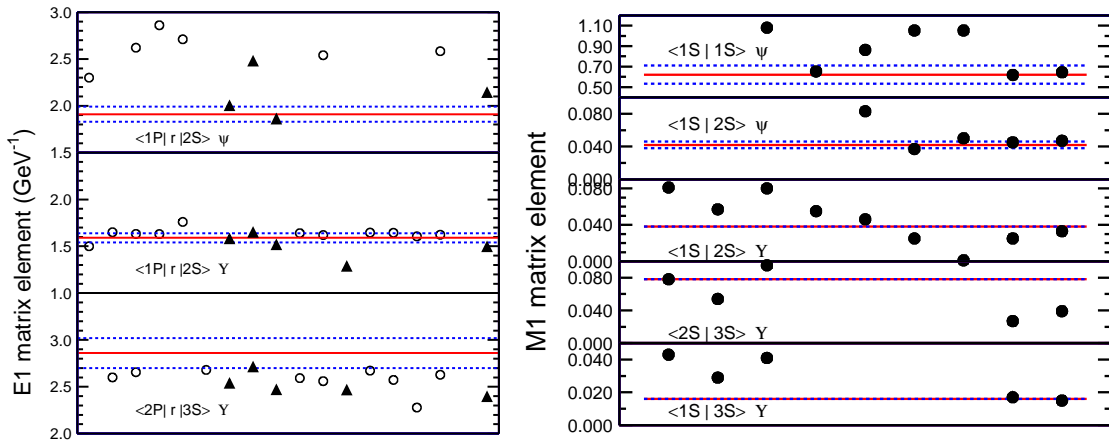


Figure 4: Measured and predicted values of matrix elements for: (a) E1 (left), and (b) M1 (right) transitions in heavy quarkonia. The E1 rates are averaged over different spins of the triplet P states. The measured values are calculated from the CLEO branching ratio results (and total widths of the triplet S states^{6,14}), except for the direct M1 transition, $2S \rightarrow 1S$, where the world average branching ratio⁶ is used. The central values and error bars for the measured values are indicated by the solid and dashed lines respectively. The solid lines for the M1 transitions in the Υ system show the experimental upper limits. Circles (triangles) show non-relativistic (relativistic) calculations. The relativistic calculations are averaged over spins with the same weights as the data.

The predictions¹⁵ are ordered according to the publication date.

Acknowledgments

The author thanks his CLEO colleagues for the input to this article. This work was supported by the National Science Foundation and the U.S. Department of Energy.

References

1. CLEO Collaboration, Y. Kubota *et al.*, *Nucl. Instrum. Meth. A* **320**, 66 (1992); G. Viehhauser *et al.*, *Nucl. Instrum. Meth. A* **462**, 146 (2001); D. Peterson *et al.*, *Nucl. Instrum. Meth. A* **478**, 142 (2002).
2. M. Artuso *et al.*, *Nucl. Instrum. Meth. A* **502**, 91 (2003).
3. R704 Collaboration, C. Baglin *et al.*, *Phys. Lett. B* **171**, 135 (1986); E760 Collaboration, T. A. Armstrong *et al.*, *Phys. Rev. Lett.* **69**, 2337 (1992).
4. S. Godfrey, J.L. Rosner, *Phys. Rev. D* **66**, 014012 (2002); D. Joffe, Ph.D. thesis, Northwestern University, 2004.
5. CLEO Collaboration, N. E. Adam *et al.*, arXiv:hep-ex/0503028.
6. Particle Data Group, S. Eidelman *et al.*, *Phys. Lett. B* **592**, 1 (2004).
7. BES Collaboration, M. Ablikim *et al.*, *Phys. Rev. D* **70**, 012003 (2004).
8. E835 Collaboration, M. Andreotti *et al.*, *Phys. Rev. D* **71**, 032006 (2005).
9. CLEO Collaboration, M. Artuso *et al.*, *Phys. Rev. Lett.* **94**, 032001 (2005); S. B. Athar *et al.*, *Phys. Rev. D* **70**, 112002 (2004).
10. P. Moxhay, J. L. Rosner, *Phys. Rev. D* **28**, 1132 (1983); R. McClary, N. Byers, *Phys. Rev. D* **28**, 1692 (1983).
11. Crystal Ball Collaboration, J.E. Gaiser *et al.*, *Phys. Rev. D* **34**, 711 (1986).
12. Crystal Ball Collaboration, C. Edwards *et al.*, *Phys. Rev. Lett.* **48**, 70 (1982).
13. Belle Collaboration, S.K. Choi *et al.*, *Phys. Rev. Lett.* **89**, 102001 (2002); CLEO Collaboration, D.M. Asner *et al.*, *Phys. Rev. Lett.* **92**, 142001 (2004); BaBar Collaboration, B. Aubert *et al.*, *Phys. Rev. Lett.* **92**, 142002 (2004).
14. CLEO Collaboration, G.S. Adams *et al.*, *Phys. Rev. Lett.* **94**, 012001 (2005).
15. The following sample of potential model predictions for the E1 matrix elements (ordered according to the publication date) is displayed in Fig. 4a: D. Pignon, C. A. Piketty, *Phys. Lett. B* **74**, 108 (1978); E. Eichten, K. Gottfried, T. Kinoshita, K. D. Lane, T. M. Yan, *Phys. Rev. D* **21**, 203 (1980); W. Buchmuller, G. Grunberg, S.-H. Tye *Phys. Rev. Lett.* **45**, 103 (1980), *Phys. Rev. D* **24**, 132 (1981); C. Quigg, J. L. Rosner, *Phys. Rev. D* **23**, 2625 (1981) (2 entries: $c\bar{c}$, $b\bar{b}$ potential respectively); J. Baacke, Y. Igarashi, G. Kasperidus, *Z. Phys. C* **13**, 131 (1982); R. McClary, N. Byers, *Phys. Rev. D* **28**, 1692 (1983); P. Moxhay, J. L. Rosner, *Phys. Rev. D* **28**, 1132 (1983); H. Grotch, D. A. Owen, K. J. Sebastian, *Phys. Rev. D* **30**, 1924 (1984); S. N. Gupta, S. F. Radford, W. W. Repko, *Phys. Rev. D* **26**, 3305 (1982), *Phys. Rev. D* **30**, 2424 (1984); S. N. Gupta, S. F. Radford, W. W. Repko, *Phys. Rev. D* **34**, 201 (1986); M. Bander, D. Silverman, B. Klima, U. Maor, *Phys. Lett. B* **134**, 258 (1984), *Phys. Rev. D* **29**, 2038 (1984), *Phys. Rev. D* **36**, 3401 (1987); W. Kwong, J. L. Rosner, *Phys. Rev. D* **38**, 279 (1988); L. P. Fulcher, *Phys. Rev. D* **37**, 1259 (1988); S. N. Gupta, W. W. Repko, C. J. Suchyta III, *Phys. Rev. D* **39**, 974 (1989); L. P. Fulcher, *Phys. Rev. D* **42**, 2337 (1990); A. K. Grant, J. L. Rosener, E. Rynes, *Phys. Rev. D* **47**, 1981 (1993); T. A. Lahde, *Nucl. Phys. A* **714**, 183 (2003). The following sample of potential model predictions for the M1 matrix elements (ordered according to the publication date) is displayed in Fig. 4b: V. Zambetakis, N. Byers, *Phys. Rev. D* **28**, 2908 (1983); H. Grotch, D. A. Owen, K. J. Sebastian, *Phys. Rev. D* **30**, 1924 (1984) (2 entries: scalar and vector confinement potential); S. Godfrey, N. Isgur, *Phys. Rev. D* **32**, 189 (1985) (2 entries: based on quoted transition moments and wave functions, respectively); X. Zhang, K. J. Sebas-

tian, H. Grotch, *Phys. Rev. D* **44**, 1606 (1991) (2 entries: scalar-vector and pure scalar confinement potential); D. Ebert, R. N. Faustov, V. O. Galkin *Phys. Rev. D* **67**, 014027 (2003); T. A. Lahde, *Nucl. Phys. A* **714**, 183 (2003). Values of the M1 matrix elements in the $b\bar{b}$ system are displayed for the photon energies and b quark mass assumed in S. Godfrey, J. L. Rosner, *Phys. Rev. D* **64**, 074011 (2001), Erratum-ibid. **65**, 039901 (2002).